The effect of sulforaphane on the cell cycle, apoptosis and expression of cyclin D1 and p21 in the A549 non-small cell lung cancer cell line

AGNIESZKA ŻURYŃ[1], ANNA LITWINIEC[2], BARBARA SAFIEJKO-MROCZKA[3], ANNA KLIMASZEWSKA-WIŚNIEWSKA[1], MACIEJ GAGAT[1], ADRIAN KRAJEWSKI[1], LIDIA GACKOWSKA[4] and DARIUSZ GRZANKA[5]

[1]Department of Histology and Embryology, Nicolaus Copernicus University in Toruń, Collegium Medicum in Bydgoszcz, Faculty of Medicine, 85-092 Bydgoszcz; [2]Plant Breeding and Acclimatization Institute - National Research Institute, Bydgoszcz Research Center, Department of Genetics and Breeding of Root Crops, Laboratory of Biotechnology, 85-090 Bydgoszcz, Poland; [3]Department of Biology, The University of Oklahoma, Norman, OK 73019-4105, USA; Departments of [4]Immunology and [5]Dermatology, Sexually Transmitted Diseases and Immunodermatology, Nicolaus Copernicus University in Toruń, Collegium Medicum in Bydgoszcz, Faculty of Medicine, 85-094 Bydgoszcz, Poland

Received January 14, 2016; Accepted February 20, 2016

DOI: 10.3892/ijo.2016.3444

Abstract. Sulforaphane (SFN) is present in plants belonging to *Cruciferae* family and was first isolated from broccoli sprouts. Chemotherapeutic and anticarcinogenic properties of sulforaphane were demonstrated, however, the underlying mechanisms are not fully understood. In this study we evaluated the expression of cyclin D1 and p21 protein in SFN-treated A549 cells and correlated these results with the extent of cell death and/or cell cycle alterations, as well as determined a potential contribution of cyclin D1 to cell death. A549 cells were treated with increasing concentrations of SFN (30, 60 and 90 μM) for 24 h. Morphological and ultrastructural changes were observed using light, transmission electron microscope and videomicroscopy. Image-based cytometry was applied to evaluate the effect of SFN on apoptosis and the cell cycle. Cyclin D1 and p21 expression was determined by flow cytometry, RT-qPCR and immunofluorescence. siRNA was used to evaluate the role of cyclin D1 in the process of suforaphane-induced cell death. We found that the percentage of cyclin D1-positive cells decreased after the treatment with SFN, but at the same time mean fluorescence intensity reflecting cyclin D1 content was increased at 30 μM SFN and decreased at 60 and 90 μM SFN. Percentage of p21-positive cells increased following the treatment, with the highest increase at 60 μM SFN, at which concentration mean fluorescence intensity of this protein was also significantly increased. The 30-μM dose of SFN induced an increased G2/M phase population along with a decreased polyploid fraction of cells, which implies a functional G2/M arrest. The major mode of cell death induced by SFN was necrosis and, to a lower degree apoptosis. Transfection with cyclin D1-siRNA resulted in significantly compromised fraction of apoptotic and necrotic cells, which suggests that cyclin D1 is an important determinant of the therapeutic efficiency of SFN in the A549 cells.

Correspondence to: Dr Dariusz Grzanka, Department of Dermatology, Sexually Transmitted Diseases and Immunodermatology, Nicolaus Copernicus University in Toruń, Collegium Medicum in Bydgoszcz, Faculty of Medicine, Karłowicza 24, 85-094 Bydgoszcz, Poland
E-mail: d_gr@me.com

Key words: cyclin D1, p21, A549, sulforaphane, cell death

Introduction

Sulpforaphane [SFN; 1-isotiocyanato-4-(methylsulfinyl) butane] was first isolated from broccoli sprouts and at high concentrations is present in plants belonging to *Cruciferae* family (1). It is believed to be a potent chemopreventive agent and was proved to activate phase II detoxification enzymes including glutathione S-transferase, epoxide hydrolase, quinone reductase and UDP-glucuronosyltransferase, but also to suppress phase I drug metabolism enzymes, which may contribute to simultaneous enhanced cellular excretion and inhibition of carcinogens (2). Chemotherapeutic and anticancerogenic capacities of the agent were demonstrated *in vitro* by inhibition of cancer cell proliferation as well as *in vivo* in a broad range of animal cancer models, including rodent carcinogenesis models of lung, mammary gland, stomach, colon and bladder cancers (3-9). However, the mechanisms of sulforaphane anticancer actions are not fully understood at present.

The $p21^{WAF1/CIP1}$ protein belongs to the Cip/Kip family of Cdk (cyclin-dependent kinase) inhibitors, participating in cell

cycle control via inhibition of the G1 cyclin-Cdk complexes and maintenance of retinoblastoma tumor suppressor protein (Rb) in its hypophosphorylated state (10-13). This tumor suppressor mediates p53 activity in the execution of G1 and G2 cell cycle arrest (14-16). Alterations of p21 and its function may contribute to an unfavorable prognosis in primary solid tumors and to development of a drug-resistance phenotype (17-19). Loss of functional p21 along with p53 may result in unrestrained cell cycle progression to the S phase despite the presence of DNA damage, leading to genomic instability and carcinogenesis.

Cyclin D1 is a protein involved in the G1/S cell cycle progression, via its participation in complexes with cyclin-dependent kinases cdk4, cdk6 and, as a consequence Rb phosphorylation and inhibition of its function (20-22). In this context, the role of cyclin D1 seems to be opposite to p21 and the protein was defined as a protooncogene. In fact, increased levels of cyclin D1 and/or its gene amplification were reported in many neoplasms and may be related to cancer cell-specific alterations of the cell cycle and neoplastic transformation (23).

Our previous study suggested that cyclin D1 expression in the A549 non-small cell lung carcinoma cell line may constitute an important determinant of the treatment efficiency (24). Other studies also emphasize the role of this protein, as its downregulation via siRNA approach resulted in inhibition of proliferation, invasion and metastasis of A549 cells *in vitro* and *in vivo* (25).

The objective of this study was to evaluate cyclin D1 and p21 expression in the A549 cells treated with sulforaphane as well as to investigate a potential involvement of cyclin D1 in the therapeutic outcome of SFN treatment by using cyclin D1-targeting siRNA. Our studies show a significant role of cyclin D1 in cell death induction in A549 SFN-treated cells.

Materials and methods

Cell culture and SFN treatment. The human non-small cell lung carcinoma cell line A549 was kindly provided by Dr P. Kopiński (Department of Gene Therapy, Ludwik Rydygier Collegium Medicum in Bydgoszcz, Nicolaus Copernicus University in Toruń, Poland) and by Dr Rajagopal Ramesh (Department of Pathology, Stanton L. Young Biomedical Research Center, University of Oklahoma Health Sciences Center, Oklahoma City, OK, USA). The cells were cultured in monolayers at 37˚C in a humidified CO_2 incubator (5% CO_2) in DMEM (Gibco) supplemented with 10% fetal bovine serum (FBS; Gibco) and 50 μg/ml of gentamycin (Sigma-Aldrich). Twenty-four hours after seeding, the cells were treated with sulforaphane (Sigma-Aldrich) (30, 60 and 90 μM) for 24 h, and the following experimental procedures were performed.

siRNA transfection. For the nucleofection of A549 cells a total of $1x10^6$ cells were transfected using SE Cell Line 4D-Nucleofector X kit according to the manufacturer's instructions. Briefly, the cells were suspended in 100 μl SE Nucleofector solution containing 3 pmol siRNA against human CCND1 (corresponding to sequence: 5'-AAG GCC AGT ATG ATT TAT AAA-3'; Qiagen, Hilden, Germany). Then, the mixture was transferred into transfection cuvettes. The electroporation was done using 4D-Nucleofector device (Lonza, Verviers, Belgium) under the program CM-130. As a negative control, the commercially designed AllStars negative control siRNA (Qiagen) was used. After transfection, the cells were grown in medium without antibiotics for 72 h and then they were used for further experiments.

Videomicroscopy. Seven thousand (7,000) cells suspended in 2 ml of CDMEM were seeded onto 25-mm cover glasses in cell culture dishes and incubated for 24 h to allow the cells to spread and form adhesions to the substratum. Then cells on the 25-mm cover glasses were transferred to a perfusion filming chamber and were then placed on the stage of a Zeiss phase-contrast microscope fitted with camera. The digital images of cells were recorded every thirty seconds on the computer drive using Scion software to obtain a time lapse recordings of individual cells. Cells were filmed in the presence of CDMEM alone for 25 min (50 frames) to observe normal cell behavior. After 25 min, CDMEM was changed to CDMEM containing sulforaphane at concentrations 30, 60 and 90 μM and recorded for an additional 350 frames. Videos were then analyzed qualitatively to determine the effects of sulforaphane on the cells.

Transmission electron microscopy (TEM). Conventional electron microscopy was used to visualize A549 cell morphology at the ultrastructural level. The cells were washed with sodium cacodylate buffer and fixed in 3.6% glutaraldehyde (pH 7.2, Merck) (30 min, RT). After washing in 0.1 M sodium cacodylate buffer (pH 7.4; Sigma-Aldrich), the cells were postfixed in 1% buffered OsO_4 for 1 h, dehydrated in ethanol (30-90%) and acetone (90-100%) and embedded in Epon E812 (Roth). Semithin sections were stained with 1% toluidine blue and used for targeting the cells. Ultrathin sections (40-nm thick) were double-stained with uranyl acetate (Chemapol) and lead citrate (BDH England). The material was examined using a transmission electron microscope JEM 100 CX (Jeol, Tokyo, Japan) operating at 60 kV cell images were recorded on IMAGO - EM23 film (NDT System, Warsaw, Poland).

Trypan blue dye exclusion test. Trypan blue dye exclusion method was used to determine the number of dead and viable cells. The cells were trypsinized and 10 μl of cell suspension was added to an equal volume of diluted trypan blue stain (Sigma-Aldrich). The number of stained cells and total number of cells were determined using Bürker counting chamber.

Annexin V/propidium iodide (PI) binding assay. To assess the mode of cell death, the Tali® Apoptosis kit - Annexin V Alexa Fluor® 488 and propidium iodide (Invitrogen) was used according to the manufacturer's instructions. In short, after the SFN treatment, the cells were collected from 6-well plates using trypsin-EDTA solution, centrifuged at 300 x g for 8 min, resuspended in ABB (Annexin V binding buffer) and incubated with Annexin V Alexa Fluor 488 at room temperature in the dark for 20 min. Following the centrifugation at 300 x g for 5 min, the cells were again resuspended in ABB and incubated with propidium iodide at room temperature in the dark for 5 min. The cells were examined using a Tali®

Image-Based Cytometer (Invitrogen). The data were analyzed by FCS Express Research Edition software (version 4.03; De Novo Software, New Jersey, NJ, USA) and expressed as the percentage of cells in each population (viable Annexin V^-/PI^-; early apoptotic Annexin V^+/PI^-; late apoptotic Annexin V^+/PI^+; necrotic Annexin V^-/PI^+).

DNA content analysis. For DNA content analysis, the Tali® Cell Cycle kit (Invitrogen) was used according to the manufacturer's instructions. Briefly, the cells were harvested from 6-well plates by trypsinization, rinsed with PBS, fixed in ice-cold 70% ethanol at 4˚C, and left at -25˚C overnight. The cells were then centrifuged at 1,000 x g for 5 min at 4˚C and washed with PBS. After centrifugation at 500 x g for 10 min at 4˚C, the cells were resuspended in Tali® Cell Cycle Solution containing propidium iodide (PI), RNase A, and Triton® X-100. Following 30-min incubation at RT in the dark, the cells were analyzed using Tali® Image-Based Cytometer (Invitrogen) and the percentage of cells in each phase of cell cycle was determined using FCS Express Research Edition software (version 4.03; De Novo Software, NJ, USA).

Flow cytometric analysis of cyclin D1 and p21 expression. Cells grown in 6-well plates were harvested, washed with PBS, centrifuged (5 min, 300 x g) and fixed with 1% methanol-free, ultra pure formaldehyde (Polysciences, Inc.). After incubation on ice (15 min in the dark) and subsequent centrifugation (5 min, 300 x g), the cells in pellets were permeabilized by the addition of 1 ml of ice-cold 50% (v/v) methanol (JT Baker) for 30 min on ice, washed twice with cold PBS and resuspended in 0.5% bovine serum albumin (BSA; Sigma-Aldrich). For intracellular staining, the cell suspensions were transferred into flow cytometric tubes containing 20 μl of FITC conjugated mouse anti-human cyclin D1 (BD Pharmingen) or Alexa Fluor 488 conjugated mouse monoclonal anti-human p21 (Santa Cruz Biotechnology, Inc.), and 200 μl of 0.5% BSA. Following a 45-min incubation (4˚C, in the dark) and washing with PBS, the cells were centrifuged (5 min, 500 x g) to wash off excess antibody and resuspended in 200 μl of PBS for flow cytometric analysis on FACScan (Becton-Dickinson). CellQuest software (Becton-Dickinson) was used to calculate the percentage of cyclin D1-positive cells, and their mean fluorescence intensity.

RT-qPCR analysis of cyclin D1 and p21 expression. To determine the expression level of p21 and cyclin D1, SYBR green-based and probe-based RT-qPCR assays, respectively, were performed using LightCycler 2.0 Instrument (Roche Applied Science) and LightCycler Software Version 4.0. In the case of SYBR green-based assays, total RNA from the A549 cells was prepared using the Total RNA kit (A&A Biotechnology; Gdynia, Poland) according to the manufacturer's protocol. Then, the reverse transcription and qPCR reactions were carried out in a single 20-μl LightCycler capillary (Roche Applied Science) as a one-step RT-qPCR with TranScriba reverse transcriptase and Master Mix SYBR (TranScriba-qPCR Master Mix SYBR kit; A&A Biotechnology) and a pair of gene-specific primers (forward; 5'-GCATGACAGATTTCTACCACTCC-3'; reverse 5'-AAGATGTAGAGCGGGCCTTT-3'), as specified by the manufacturer. The total reaction mixture (20 μl) contained 60 ng of RNA and 0.2 μM of each primer in addition to the TranScriba-qPCR Master Mix SYBR kit components. One cycle of reverse transcription was carried out for 10 min at 50˚C, one cycle of denaturation for 3 min at 95˚C, and 43 cycles of denaturation for 15 sec at 95˚C, followed by annealing and elongation for 30 sec at 57˚C.

In turn, a two-step real-time RT-qPCR was performed to assess the expression level of cyclin D1. The preparation of cell lysate was done with RealTime ready Cell Lysis kit (Roche Applied Science) according to the manufacturer's instructions. The resulting lysate was directly reverse transcribed using Transcriptor Universal cDNA Master (Roche Applied Science) following the manufacturer's instructions in a final volume of 20 μl (2 μl of the total lysate/cDNA reaction). Reverse transcription was carried out for 10 min at 55˚C, followed by incubation at 85˚C for 5 min. Synthesized cDNA was stored at -20˚C until further use. RT-qPCRs were conducted with the LightCycler TaqMan Master kit (Roche Applied Science) in LightCycler capillaries in a 20-μl reaction volume. PCR reaction mixture contained: 5 μl of cDNA, 1X TaqMan Master mix, 400 nM of each primer for the examined gene (forward 5'-TGTCCTACTACCGCCTCACA-3'; reverse 5'-CAGGGCTTCGATCTGCTC-3'), 400 nM Primer mix for the reference gene (Human PBGD Gene assay; Roche Applied Science, cat. no. 05 046 149 001), 200 nM of each hydrolysis TaqMan probe for the examined (#16; Roche Applied Science, cat. no. 04 686 896 001) and reference (Human PBGD Gene assay; Roche Applied Science, cat. no. 05 046 149 001) genes and PCR-grade H_2O to adjust to the final reaction volume. Thermocycling conditions consisted of 10 min of initial denaturation at 95˚C, followed by 45 cycles of denaturation at 95˚C for 10 sec, annealing at 60˚C for 30 sec and extension at 72˚C for 1 sec with a single fluorescence acquisition step at the end of extension, followed by final cooling at 40˚C for 30 sec. Relative mRNA expression levels of p21 and cyclin D1 were quantified using the ΔΔCt method ($2^{-\Delta\Delta Ct}$ method) (26) and the results were normalized to the expression of the housekeeping gene glyceraldehyde-3-phosphate dehydrogenase (GAPDH) or porphobilinogen deaminase (PBGD), respectively, and presented as a fold difference relative to a calibrator sample (untreated A549 cells).

Cyclin D1 and p21 immunofluorescence. A549 cells growing on coverslips were briefly washed with PBS, fixed in 4% paraformaldehyde (15 min, RT) and then washed with PBS (3x5 min). After that, the cells were incubated in permeabilization solution (0.1% Triton X-100 in PBS) and blocked with 1% BSA. After permeabilization, the cells were incubated with mouse monoclonal anti cyclin D1 antibody (Sigma-Aldrich) or mouse monoclonal anti-p21 antibody (Santa Cruz Biotechnology Inc), respectively (60 min, RT), washed three times with PBS and incubated with Alexa Fluor 488 goat anti-mouse IgG (Invitrogen, Molecular Probes) (60 min, in the dark). Nuclear staining was performed with DAPI (Sigma-Aldrich). After incubation, the cells were washed with PBS and then mounted on microscope slides in Aqua Poly/Mount (Polysciences, Inc.). Both cyclin D1 or p21 and DAPI staining were examined using a Nikon Eclipse E800 fluorescence microscope (Nikon; Tokyo, Japan) and NIS-Elements 4.0 software (Nikon).

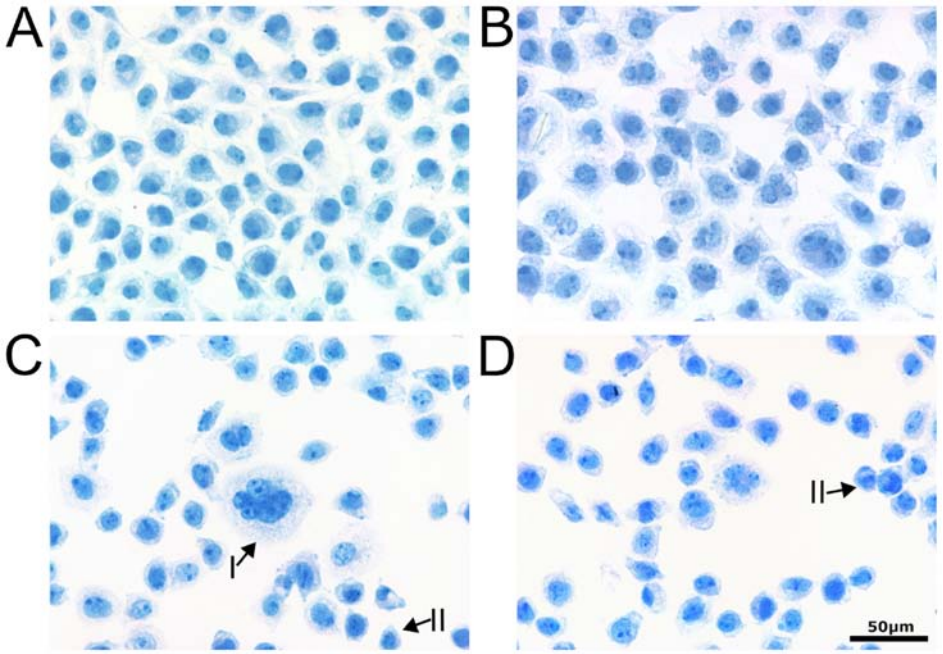

Figure 1. Morphology of A549 cells treated with sulforaphane. (A) Control cells. (B) Cells treated with 30 μM SFN. (C) Cells treated with 60 μM SFN. (D) Cells treated with 90 μM SFN. Bar, 50 μm. Cell with micronuclei (I) and shrunken cells (II) were observed.

Statistical analysis. The analysis was performed using statistical software (GraphPad Prism, San Diego, CA, USA). The data were compared by the nonparametric Mann-Whitney U test and the changes were considered statistically significant at the level of $p<0.05$.

Results

Cell morphology

Hematoxylin staining. Control cells and the cells treated with 30 μM SFN were regular in shape, displayed visible oval nucleus and nucleoli. Incubation with higher doses of sulforaphane resulted in cytoplasmic vacuolization and appearance of enlarged cells with micronuclei, most probably displaying features of mitotic catastrophe. Some of the cells were shrunken, with condensed chromatin in the nucleus, suggesting early apoptosis (Fig. 1).

Videomicroscopy. In order to observe cell response to sulforaphane treatment, representative groups of cells were recorded by videomicroscopy. Cells were observed for 25 min before introduction of SFN to the cell environment. In control conditions (cell culture medium) cells were actively protruding and withdrawing cell edges around cell periphery for the entire time of recording (200 min for control and 25 min for SFN-treated cells). After replacing the growth medium with medium containing sulforophane, we observed the dose- and time-dependent cell response to SFN. Cells exposed to 30 μM SFN developed short microspikes and densities around cell periphery and on cell dorsal surface. Observed cells were gradually shrinking as time of SFN exposure progressed. Cell response was stronger and occurred faster in higher concentrations of SFN. At both 60 and 90 μM SFN, cells developed longer microspikes and were withdrawing and retracting from cell edges all over the cell periphery. Eventually cells rounded up at about three hours of SFN treatment and were completely rounded and detached from each other at 90 μM sulforaphane (Fig. 2).

Transmission electron microscopy. Transmission electron microscopy analysis revealed the presence of ultrastructural alterations in A549 cells, which appeared as a result of incubation with sulforaphane. The control cells displayed regular oval shape with prominent nucleus, distinct nucleolus and maintained the integrity of cellular membranes (Fig. 3A). The cells treated with 30 μM sulforaphane featured significant cytoplasmic vacuolization as compared to control. Changes in the nuclear morphology were also evident (Fig. 3B). Appearance of large vacuoles and lysosome-like structures, as well as swollen mitochondria were induced by 60 μM sulforaphane. The cell nucleus at this concentration was shrunken, with unrecognizable nucleolus (Fig. 3C). At the highest sulforaphane concentration, i.e., 90 μM, the cells manifested irregularities in shape and prominent vacuolization, often comprising the whole cytoplasmic area. Other typical features included chromatin condensation and disappearance of nucleoli (Fig. 3D).

Cell death/survival

Trypan blue dye exclusion test. A dose-dependent decrease in the number of viable A549 cells was found as a result of sulforaphane treatment. Along with increasing SFN concentrations, 30, 60 and 90 μM, statistically significant differences were observed in the cell survival, with the respective median values reaching 98.4, 88 and 77.4% of the population.

Annexin V assay. After treatment with all the concentrations of sulforaphane used in this study the percentage of living

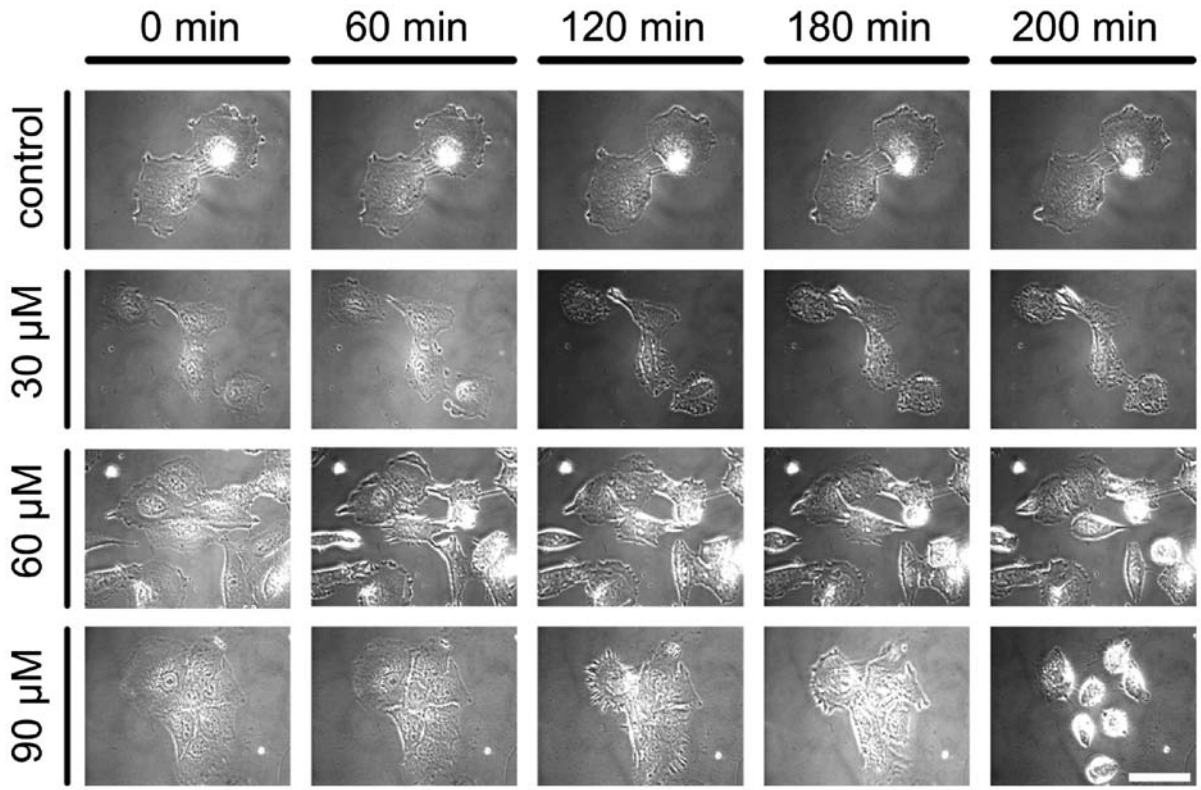

Figure 2. Live A549 cells treated with sulforaphane recorded using digital video microscopy: 0-25 min before and (30-200 min) after SFN introduction. SFN (30 μM) induced only slight changes in cells shape due to cell edge withdrawal, while higher concentrations of SFN resulted in leading edge alterations, appearance of microspikes and cell shrinkage. After longer treatment with 60 μM of SFN (180-200 min) and 90 μM of SFN (180-200 min) cells rounded up.

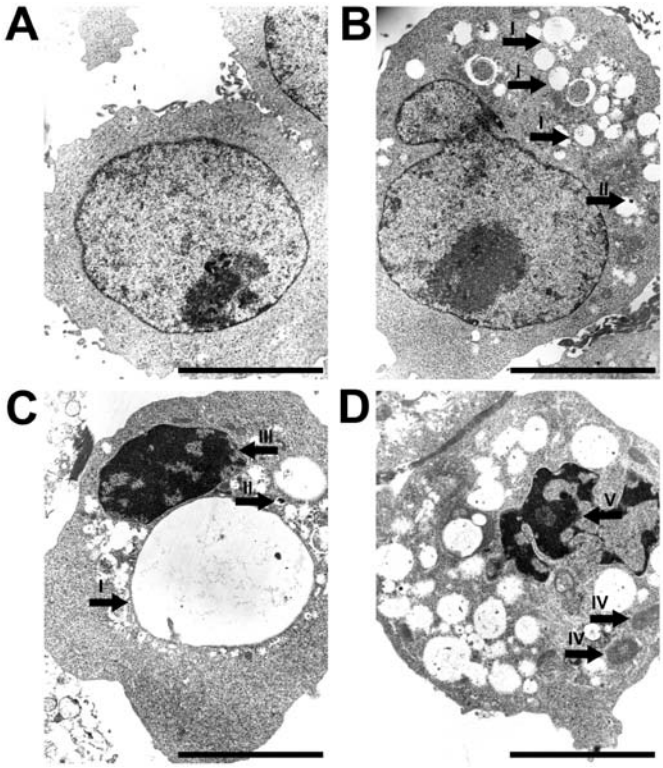

Figure 3. Ultrastructure of A549 cells treated with sulforaphane. (A) Control cells. (B) Cells treated with 30 μM SFN. (C) Cells treated with 60 μM SFN. (D) Cells treated with 90 μM SFN. Bar, 5 μm. Hypervacuolization (I), lysosome-like structures (II), shrunken nucleus (III), swollen mitochondria (IV) and disintegration of nucleus (V) were observed in sulforaphane-treated cells.

cells decreased (Mann-Whitney U, $p<0.05$) (Fig. 4). In non-transfected cells, the percentages of early and late apoptosis was increased at 30 μM sulforaphane as compared to the control cells, which was followed by a further decrease at higher concentrations. The tendency was reversed as far as necrosis is concerned, giving increased percentage of dead cells starting at 60 μM sulforaphane. After siRNA transfection we found decreased percentage of early and late apoptotic cells at 30 and 90 μM sulforaphane, as well as necrotic cells at 60 and 90 μM sulforaphane, as opposed to 30 μM sulforaphane, at which the percentages of necrotic cells were higher for the transfected cells (Mann-Whitney U, $p<0.05$). The survival of cells was unaffected by transfection, as we obtained higher percentages of living cells after siRNA procedure not only at 60 and 90 μM sulforaphane concentrations, but also in control cells, in which the percentages of early and late apoptotic cells were significantly reduced following transfection (Fig. 4).

Cell cycle and cell cycle regulatory proteins

Cell cycle. Cell cycle distribution was assessed using the Talli-based image cytometry. The subG1 fraction increased following the treatment with all the concentrations of sulforaphane used in the study, which was parallel with increased percentages of cell death observed by us. On the contrary, the G0/G1 phase population was compromised, with the most prominent effect resulting from 30 μM dose of the agent. Interestingly, the same concentration induced an increased G2/M phase population along with a decreased polyploid fraction of cells, which implies a functional G2/M arrest of

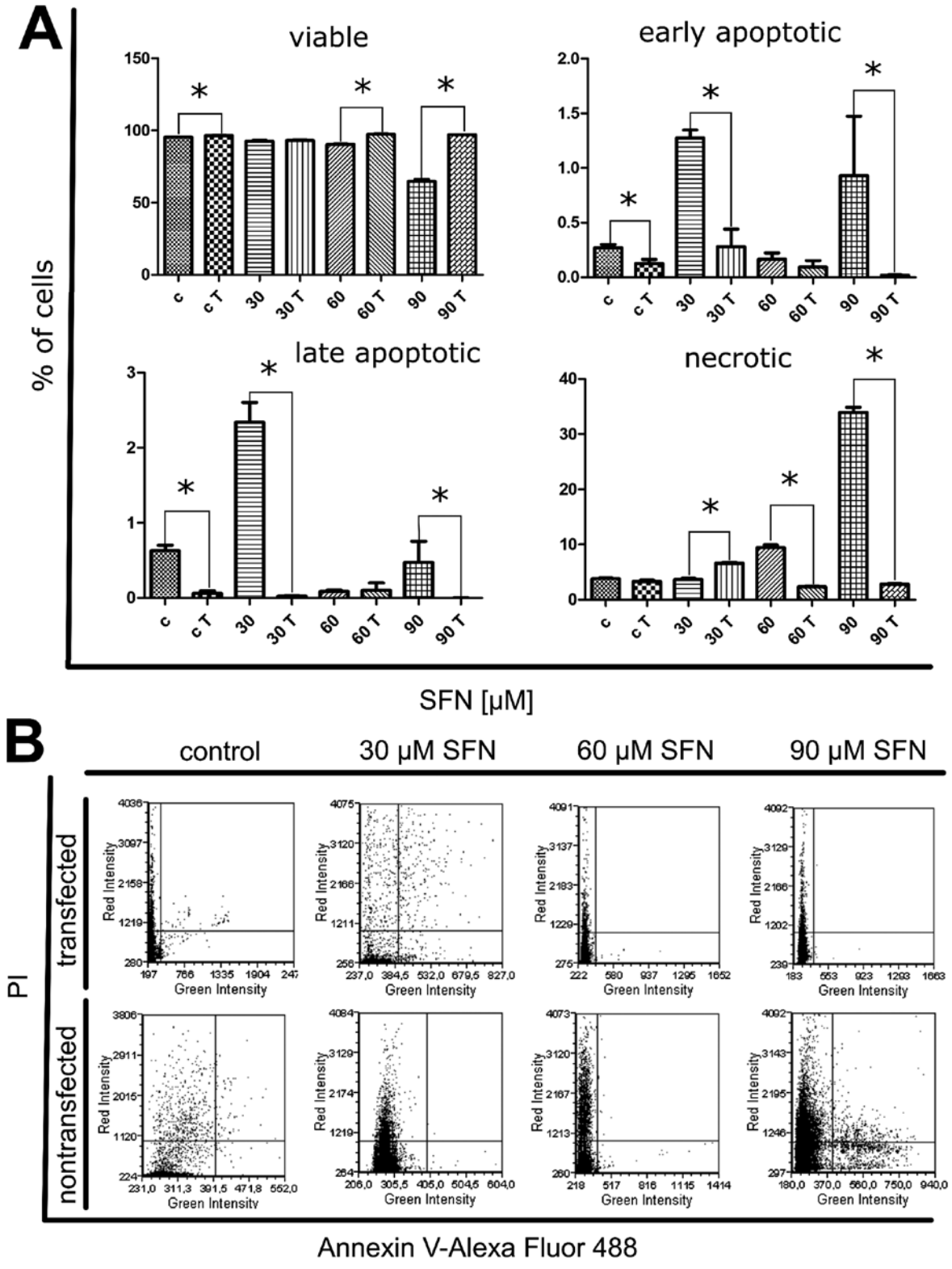

Figure 4. Image-based cytometry. Analysis of apoptosis, necrosis and cell viability - Annexin V/propidium iodide (PI) assay. (A) The percentage of viable, early apoptotic, late apoptotic, and necrotic cells in non-transfected and transfected populations. Columns, median percentage of cells; bars, interquartile range. Asterisks denote statistical significance as compared to control cells ($p<0.05$). Results are representative of five independent experiments. (B) Representative dot plots of Annexin V/PI-stained non-transfected and transfected cells (control, 30 μM SFN, 60 μM SFN and 90 μM SFN).

the cell cycle. The S phase fraction declined in turn as a result of 60 and 90 μM sulforaphane (Fig. 5).

Expression of cyclin D1. Expression of cyclin D1 after treatment with sulforaphane was changeable. RT-qPCR analysis showed that 30 and 60 μM concentrations of the drug induced an increase and 90 μM concentration induced a decrease in cyclin D1 mRNA (Mann-Whitney U test, $p<0.05$) (Fig. 6), whereas cytometric analysis revealed a slight increase in fluorescence intensity of cyclin D1 at 30 μM, followed by

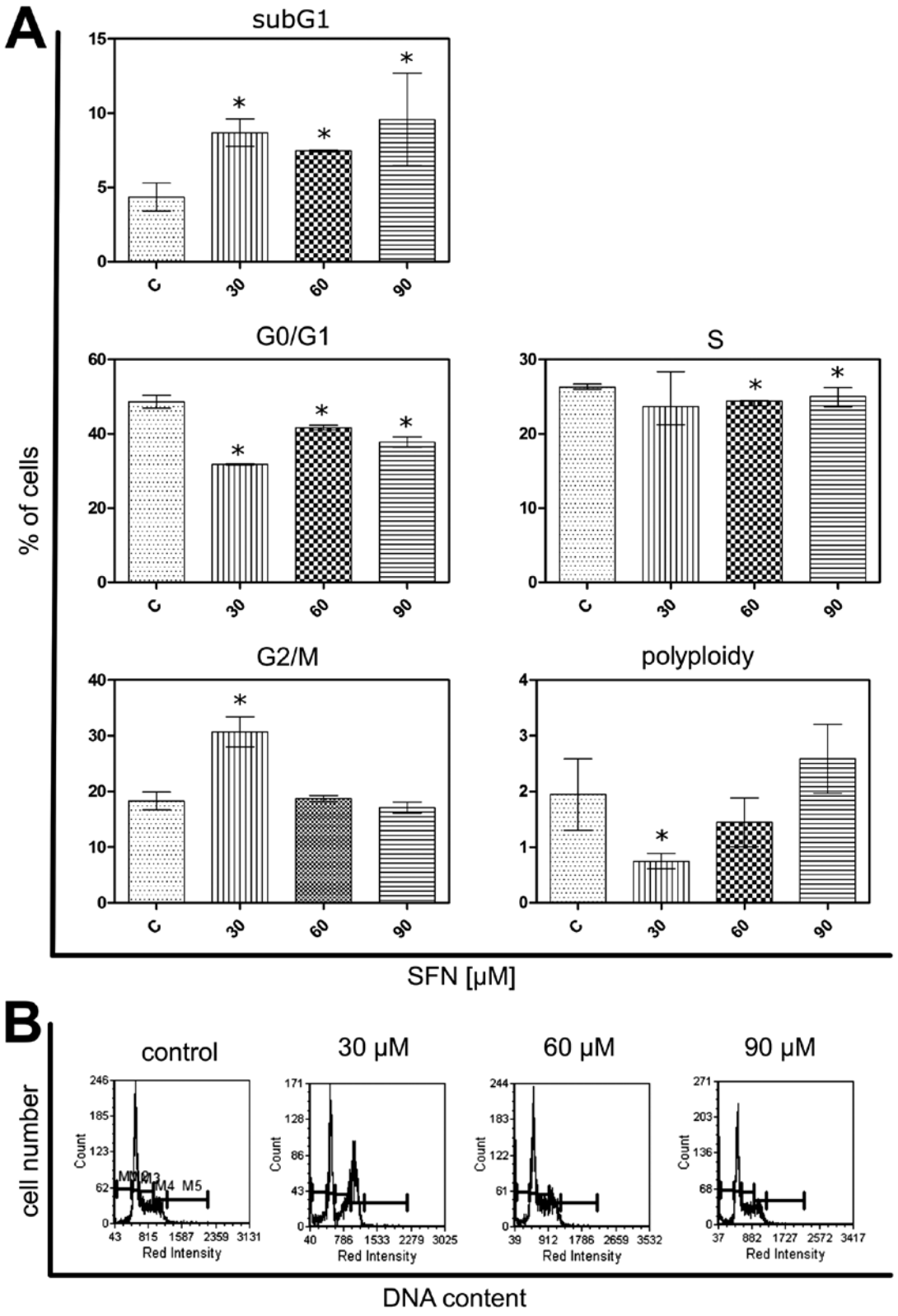

Figure 5. Image-based cytometry. Analysis of the cell cycle distribution in A549 cells treated with sulforaphane. (A) Diagrams for each of the groups defined according to DNA content are shown. Cells with DNA content corresponding to subG1 fraction, G0/G1 phases, S phase, G2/M phases and polyploidy. Columns, median percentage of cells; bars, interquartile range. Asterisks denote statistical significance as compared to control cells (Mann-Whitney U test, $p<0.05$). Results are representative of five independent experiments. (B) Representative histograms of cell cycle phases for each of the SFN doses used.

decreases at 60 and 90 μM sulforaphane. Percentages of cyclin D1-positive cells were decreased after the treatment as compared to the control cells (Mann-Whitney U test, $p<0.05$), displaying a dose-dependent tendency (Fig. 7).

Immunofluorescent labeling of cyclin D1 in SFN-treated cells showed similar tendency to flow cytometric results, i.e., the most visible increase in cyclin D1 fluorescence and nuclear localization was observed at 30 μM sulforaphane,

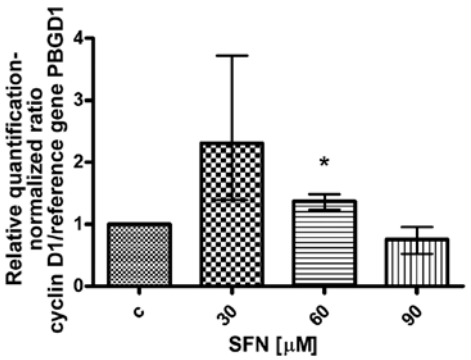

Figure 6. Real-time PCR analysis. Expression of cyclin D1 gene (*CCND1*) in relation to reference gene PBGD. Asterisks denote statistical significance as compared to control cells (Mann-Whitney U test, $p<0.05$). Columns, median percentage of cells; bars, interquartile range. Results are representative of five independent experiments.

followed by decreased expression of this protein at higher concentrations (Fig. 8).

The silencing effect of siRNA transfection on cyclin D1 expression in A549 cells was confirmed cytometrically (Fig. 7) and microscopically (Fig. 8). Slight, but significantly attenuated expression was found in control cells and after treatment with 30 μM sulforaphane.

Expression of p21. Sulforaphane induced changes in the expression of p21. RT-qPCR experiment showed significant increase of p21 mRNA after treatment with 60 μM sulforaphane, but slightly decreased levels resulting from the treatment with other doses, i.e., 30 and 90 μM SFN (Fig. 9). Flow cytometric measurements indicated that fluorescence intensity of p21 protein was increased at 60 μM SFN. At the same time, the percentage of p21-positive cells was increased

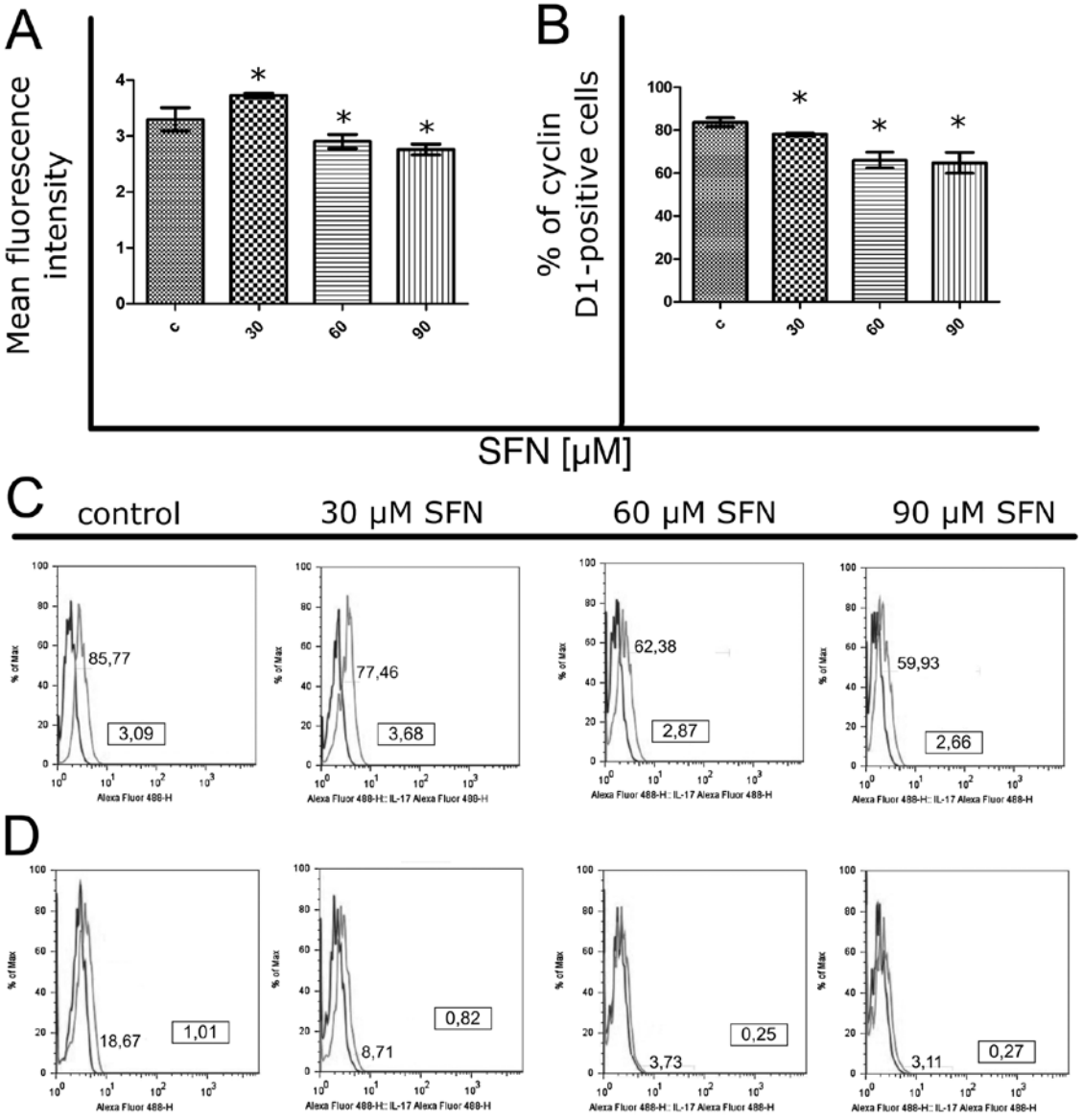

Figure 7. Flow cytometry. Analysis of cyclin D1 content in A549 cells treated with sulforaphane. (A) Mean fluorescence intensity in cyclin D1-positive population. (B) Percentage (%) of cyclin D1-positive cells. Columns, median percentage of cells; bars, interquartile range. Asterisks denote statistical significance as compared to control cells (Mann-Whitney U test, $p<0.05$). Results are representative of five independent experiments. (C) Representative histograms of the fluorescence intensity and percentages of cyclin D1-positive cells in non-transfected population. (D) Representative histograms of the fluorescence intensity and percentages of cyclin D1-positive cells in transfected population.

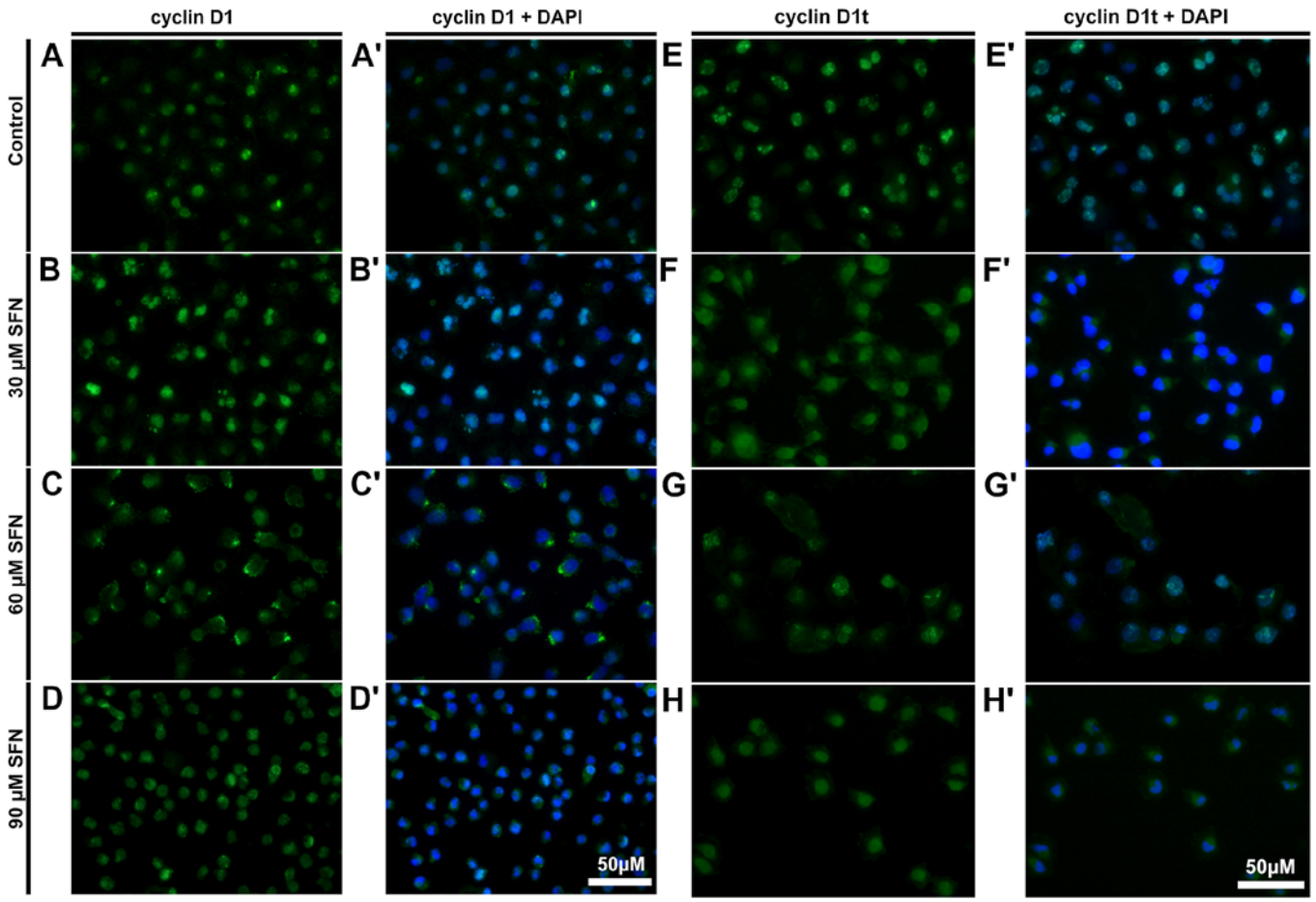

Figure 8. Fluorescence microscopy. Examination of cyclin D1 distribution in non-transfected and transfected A549 cells treated with sulforaphane. After treatment with 30, 60 and 90 μM SFN cells were immunolabeled for the presence of cyclin D1 (A-H). Cell nuclei were stained with DAPI (A'-'H'). Cyclin D1 fluorescence intensity is higher in the cell nuclei after treatment with 30 μM SFN. Fluorescence intensity was visibly compromised following cyclin D1 si-RNA approach.

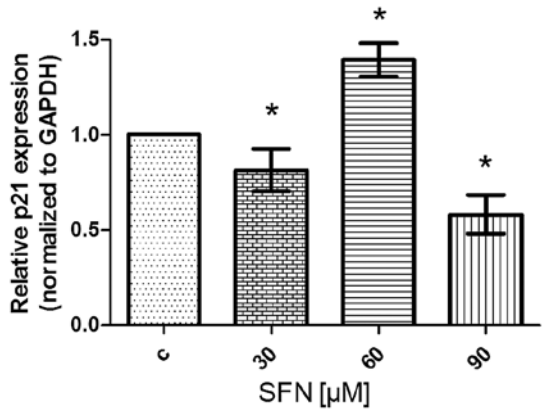

Figure 9. Real-time PCR. Analysis of p21 gene (*CDKN1A*) expression in relation to reference gene GAPDH. Asterisks denote statistical significance as compared to control cells (Mann-Whitney U test, $p<0.05$). Columns, median percentage of cells. Bars, interquartile range. Results are representative of five independent experiments.

(Mann-Whitney U test, $p<0.05$), with the most visible effect at 60 μM SFN concentration (Fig. 10).

Fluorescence microscopic examination of p21 in A549 control and SFN-treated cells suggested the most significant induction of this protein at 30 and 60 μM SFN, as the most intense labeling featured these doses (Fig. 11).

Discussion

Sulforaphane was previously shown to trigger specific cell death mechanisms in different types of cancer cells. For instance, it was demonstrated that some unique events may be typical for particular cells (27). Different apoptotic pathways, depending on a cell line were activated in response to sulforaphane in various breast cancer cell lines, i.e., in MDA-MB-231 cells induction of Fas ligand and caspase-8 and -3 cascade and poly(ADP-ribose) (PARP) was found, whereas in MDA-MB-468, MCF-7 and T47D cells reduced Bcl-2 expression, cytochrome *c* release, caspase-9 and -3 activation and PARP cleavage occurred (27). Contradictory observations appeared regarding the effects of this agent on prostate cancer cells as well (28,29). In several prostate cell lines apoptotic cell death was reported (28), but in PC-3 and LNCaP cells concomitant autophagy induction was documented, along with its consequences for cytochrome *c* release and apoptosis inhibition (29).

The role of sulforaphane (SFN) and phenethyl isothiocyanate (PEITC) as well as their molecular targets were

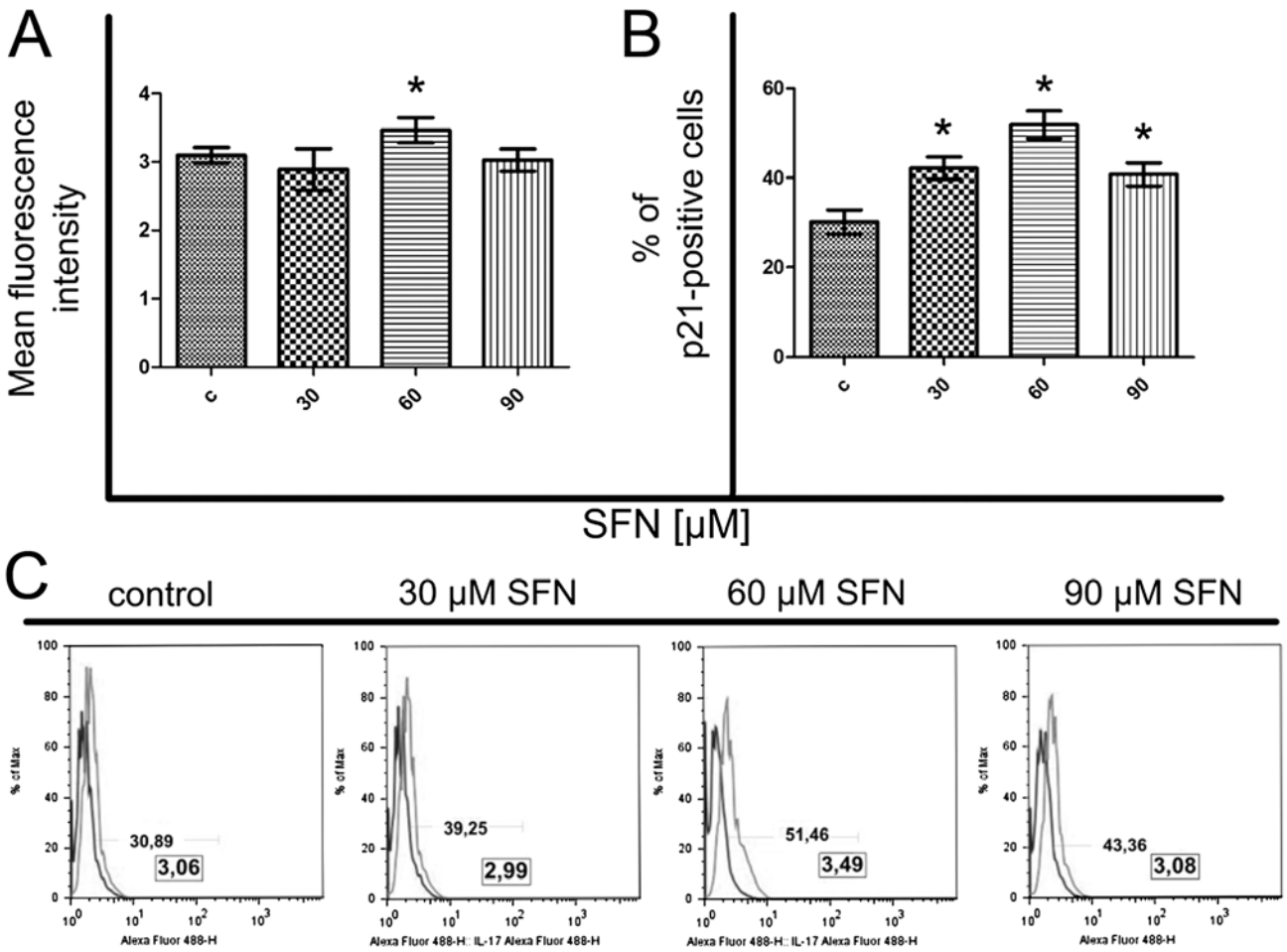

Figure 10. Flow cytometry. Analysis of p21 content in A549 cells treated with sulforaphane. (A) Mean fluorescence intensity in p21-positive population. (B) Percentage (%) of p21-positive cells. Columns, median percentage of cells; bars, interquartile range. Asterisks denote statistical significance as compared to control cells (Mann-Whitney U test, $p<0.05$). Results are representative of five independent experiments. (C) Representative histograms of the fluorescence intensity and percentages of p21-positive cells.

previously investigated in A549 non-small cell lung cancer cells (30). It was reported that sulforaphane as compared to PEITC displayed rather weak protein-binding activity, but was more potent as oxidative damage inducer in these cells (30). Cytotoxic effects of combined SFN and tumor necrosis factor-related apoptosis-inducing ligand (TRAIL) treatment were shown to be mediated by caspase-3 activation in A549 cells (31). Similarly to previous studies (30), we have found that apoptotic cells appeared starting from 30 μM SFN concentration. However, percentages of early and late apoptotic cells seemed to be low in comparison with the rate of necrosis induction, especially at higher doses, i.e., 60 and 90 μM SFN. The major cell death mode triggered in our experiment was necrosis, which was nevertheless attenuated after cyclin D1 siRNA transfection. This allows us to hypothesize that cyclin D1 may be one of the molecular targets for sulforaphane-induced necrosis in A549 cells. Interestingly, also the fraction of early and late apoptotic cells in response to SFN treatment was compromised by transfection, suggesting that cyclin D1 may be important for different modes of cell death execution in our study. Another study documented reduced viability of sulforaphane-treated ovarian cancer cell lines, which was accompanied by downregulation of cyclin D1, cdk4 and cdk6 (32). In multiple myeloma cell lines with GFP-cyclin D1 fusion protein expression it was shown that an intrinsic mitochondrial pathway of apoptosis as well as ER-dependent pathway were enhanced in response to bortezomib treatment as compared to cell lines with GFP expression (33). Concomitantly, it was documented that this effect was mediated by alterations in apoptosis/inflammation-related gene expression pattern. As also suggested by previous studies, cyclin D1 overexpression may contribute to sensitization of myeloma cells to different anti-myeloma compounds including dexamethasone, melphalan, bortezomib, and immunomodulatory thalidomide compounds, which was most probably related to a concomitant induction of the prolonged S-phase (34). Interestingly, in B-lymphoid cell lines it was found that constitutive low levels of cyclin D1 may result in delayed apoptotic response via chaperoning activity of induced Hsp70 exerted on pro-apoptotic factors (35). In this study we documented that silencing of cyclin D1 in A549 cells may result in significantly reduced necrotic cell death following SFN treatment, suggesting that this protein plays important role in modulation of not only apoptotic, but also necrotic cell death mechanisms. Recently, a role of cyclin D1 in the programmed necrotic cell death of neurons via the ROCK-p27Kip1-cyclinD1/CDK4-LIMK2-DRP1 has been

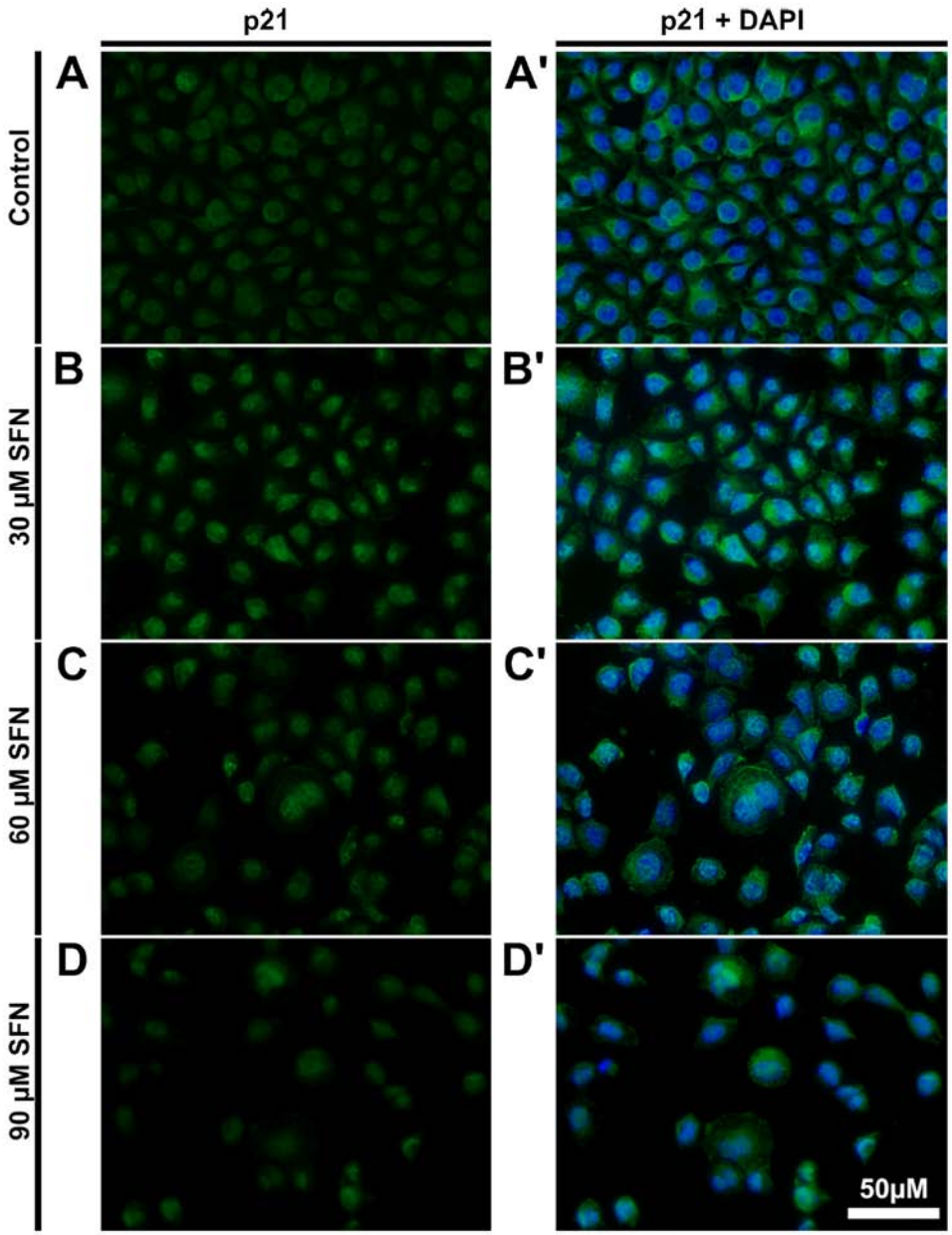

Figure 11. Fluorescence microscopy. Distribution of p21 in A549 cells treated with sulforaphane. The cells were treated with 30, 60 and 90 μM SFN and immunolabeled for the presence of p21 protein (A-D). Cell nuclei were stained with DAPI (A'-D'). p21 intensity was visibly increased following 30 and 60 μM SFN treatment especially in the nucleus.

documented to be related to mitochondrial dysfunction (36). One of the mechanisms of SFN action may be ROS generation. We observed abundant swollen mitochondria by TEM, and believe that similar pathway may be involved in necrosis induction in A549 cells by SFN.

We have previously shown that high levels of cyclin D1 may be crucial for polyploid cell appearance/stability after mitotic failure in A549 and HL-60 cells (24,37).

Furthermore, it has been suggested that one of the pathways through which SFN influences cyclin D1 may be via inhibition of NF-κB in mouse prostate cancer model (38). Moreover, downregulation of cyclin D1 in sulforaphane-treated HT-29 human carcinoma cells was proven to depend on SFN-induced oxidative stress and may be mediated by JNK pathway as well (39). In this study, a decrease of cyclin D1 protein was found resulting from 60 and 90 μM SFN as well. Besides cell death, we observed also cell cycle arrest in G2/M, which was evident at 30 μM SFN-treated cells as compared to control cells, but not at higher concentrations, suggesting cell death induction from this control point of the cell cycle.

Thus far influence of different synthetic or natural anticancer compounds on cell cycle regulatory proteins has been investigated in A549 cells, often showing downregulation of cyclin D1 and increased expression of p21, accompanying G0/G1 or G2/M cell cycle arrests and apoptotic cell death (40-45). Previous studies have shown that growth inhibitory effects of sulforaphane may also result from the G1 cell cycle arrest, which correlated with reduced cyclin D1 and p21 induction (39). p21 was shown to be an important mediator of A549 cells sensitivity to chemotherapeutic drugs (46). In this study

we also observed p21 induction at 60 μM SFN as revealed by fluorescence intensity and RT-qPCR analysis, which may be correlated with a slightly increased percentage of G0/G1 cells at this concentration as compared with the lowest SFN dose. The percentage of p21-positive cells was significantly increased by sulforaphane treatment, which also may have contributed to G2/M cell cycle arrest. However, in our study this cell cycle checkpoint seemed to be active only at the lowest dose of SFN, most probably due to enhanced cell death mechanisms at higher concentrations.

In conclusion our results indicate that the major cell death mode induced by sulforaphane in A549 cells was necrosis, which was most probably related to oxidative stress induction. Differential regulation of cell cycle proteins cyclin D1 and p21 was observed as a result of the treatment, which may be dependent on the applied concentration of SFN. Cyclin D1 seems to be an important target for regulation and determination of the outcome of the treatment, i.e., cell death induction in A549 cells, which was evident in response to SFN, but also visible in control cells, albeit to a much lower degree. To the best of our knowledge this is the first report documenting a substantial contribution of cyclin D1 to cell death, especially necrosis induction, in SFN-treated A549 cells.

Acknowledgements

This study was supported by the Nicolaus Copernicus University in Toruń, Collegium Medicum, Faculty of Medicine (grant no. 895).

References

1. Clarke JD, Dashwood RH and Ho E: Multi-targeted prevention of cancer by sulforaphane. Cancer Lett 269: 291-304, 2008.
2. Brooks JD, Paton VG and Vidanes G: Potent induction of phase 2 enzymes in human prostate cells by sulforaphane. Cancer Epidemiol Biomarkers Prev 10: 949-954, 2001.
3. Hecht SS, Kenney PM, Wang M and Upadhyaya P: Benzyl isothiocyanate: An effective inhibitor of polycyclic aromatic hydrocarbon tumorigenesis in A/J mouse lung. Cancer Lett 187: 87-94, 2002.
4. Zhang Y, Kensler TW, Cho CG, Posner GH and Talalay P: Anticarcinogenic activities of sulforaphane and structurally related synthetic norbornyl isothiocyanates. Proc Natl Acad Sci USA 91: 3147-3150, 1994.
5. Singletary K and MacDonald C: Inhibition of benzo[a]pyrene- and 1,6-dinitropyrene-DNA adduct formation in human mammary epithelial cells bydibenzoylmethane and sulforaphane. Cancer Lett 155: 47-54, 2000.
6. Fahey JW, Haristoy X, Dolan PM, Kensler TW, Scholtus I, Stephenson KK, Talalay P and Lozniewski A: Sulforaphane inhibits extracellular, intracellular, and antibiotic-resistant strains of *Helicobacter pylori* and prevents benzo[a]pyrene-induced stomach tumors. Proc Natl Acad Sci USA 99: 7610-7615, 2002.
7. Kassie F, Uhl M, Rabot S, Grasl-Kraupp B, Verkerk R, Kundi M, Chabicovsky M, Schulte-Hermann R and Knasmüller S: Chemoprevention of 2-amino-3-methylimidazo[4,5-f]quinoline (IQ)-induced colonic and hepatic preneoplastic lesions in the F344 rat by cruciferous vegetables administered simultaneously with the carcinogen. Carcinogenesis 24: 255-261, 2003.
8. Chung FL, Conaway CC, Rao CV and Reddy BS: Chemoprevention of colonic aberrant crypt foci in Fischer rats by sulforaphane and phenethyl isothiocyanate. Carcinogenesis 21: 2287-2291, 2000.
9. Verhoeven DT, Verhagen H, Goldbohm RA, van den Brandt PA and van Poppel G: A review of mechanisms underlying anticarcinogenicity by brassica vegetables. Chem Biol Interact 103: 79-129, 1997.
10. Harper JW, Adami GR, Wei N, Keyomarsi K and Elledge SJ: The p21 Cdk-interacting protein Cip1 is a potent inhibitor of G1 cyclin-dependent kinases. Cell 75: 805-816, 1993.
11. Xiong Y, Hannon GJ, Zhang H, Casso D, Kobayashi R and Beach D: p21 is a universal inhibitor of cyclin kinases. Nature 366: 701-704, 1993.
12. Denicourt C and Dowdy SF: Cip/Kip proteins: More than just CDKs inhibitors. Genes Dev 18: 851-855, 2004.
13. Gartel AL, Serfas MS and Tyner AL: p21-negative regulator of the cell cycle. Proc Soc Exp Biol Med 213: 138-149, 1996.
14. Waldman T, Kinzler KW and Vogelstein B: p21 is necessary for the p53-mediated G1 arrest in human cancer cells. Cancer Res 55: 5187-5190, 1995.
15. Wu H, Wade M, Krall L, Grisham J, Xiong Y and Van Dyke T: Targeted in vivo expression of the cyclin-dependent kinase inhibitor p21 halts hepatocyte cell-cycle progression, postnatal liver development and regeneration. Genes Dev 10: 245-260, 1996.
16. Bunz F, Dutriaux A, Lengauer C, Waldman T, Zhou S, Brown JP, Sedivy JM, Kinzler KW and Vogelstein B: Requirement for p53 and p21 to sustain G2 arrest after DNA damage. Science 282: 1497-1501, 1998.
17. Sharpless NE and DePinho RA: Telomeres, stem cells, senescence, and cancer. J Clin Invest 113: 160-168, 2004.
18. Cariou S, Donovan JC, Flanagan WM, Milic A, Bhattacharya N and Slingerland JM: Down-regulation of $p21^{WAF1/CIP1}$ or $p27^{Kip1}$ abrogates antiestrogen-mediated cell cycle arrest in human breast cancer cells. Proc Natl Acad Sci USA 97: 9042-9046, 2000.
19. Giannakakou P, Robey R, Fojo T and Blagosklonny MV: Low concentrations of paclitaxel induce cell type-dependent p53, p21 and G1/G2 arrest instead of mitotic arrest: Molecular determinants of paclitaxel-induced cytotoxicity. Oncogene 20: 3806-3813, 2001.
20. Baldin V, Lukas J, Marcote MJ, Pagano M and Draetta G: Cyclin D1 is a nuclear protein required for cell cycle progression in G1. Genes Dev 7: 812-821, 1993.
21. Sellers WR and Kaelin WG Jr: Role of the retinoblastoma protein in the pathogenesis of human cancer. J Clin Oncol 15: 3301-3312, 1997.
22. Malumbres M, Sotillo R, Santamaría D, Galán J, Cerezo A, Ortega S, Dubus P and Barbacid M: Mammalian cells cycle without the D-type cyclin-dependent kinases Cdk4 and Cdk6. Cell 118: 493-504, 2004.
23. Donnellan R and Chetty R: Cyclin D1 and human neoplasia. Mol Pathol 51: 1-7, 1998.
24. Litwiniec A, Gackowska L, Helmin-Basa A, Zuryń A and Grzanka A: Low-dose etoposide-treatment induces endoreplication and cell death accompanied by cytoskeletal alterations in A549 cells: Does the response involve senescence? The possible role of vimentin. Cancer Cell Int 13: 9, 2013.
25. Huang H, Hu YD, Li N and Zhu Y: Inhibition of tumor growth and metastasis by non-small cell lung cancer cells transfected with cyclin D1-targeted siRNA. Oligonucleotides 19: 151-162, 2009.
26. Livak KJ and Schmittgen TD: Analysis of relative gene expression data using real-time quantitative PCR and the 2(T)(-Delta Delta C) method. Methods 25: 402-408, 2001.
27. Pledgie-Tracy A, Sobolewski MD and Davidson NE: Sulforaphane induces cell type-specific apoptosis in human breast cancer cell lines. Mol Cancer Ther 6: 1013-1021, 2007.
28. Singh AV, Xiao D, Lew KL, Dhir R and Singh SV: Sulforaphane induces caspase-mediated apoptosis in cultured PC-3 human prostate cancer cells and retards growth of PC-3 xenografts in vivo. Carcinogenesis 25: 83-90, 2004.
29. Herman-Antosiewicz A, Johnson DE and Singh SV: Sulforaphane causes autophagy to inhibit release of cytochrome C and apoptosis in human prostate cancer cells. Cancer Res 66: 5828-5835, 2006.
30. Mi L, Wang X, Govind S, Hood BL, Veenstra TD, Conrads TP, Saha DT, Goldman R and Chung FL: The role of protein binding in induction of apoptosis by phenethyl isothiocyanate and sulforaphane in human non-small lung cancer cells. Cancer Res 67: 6409-6416, 2007.
31. Jin CY, Moon DO, Lee JD, Heo MS, Choi YH, Lee CM, Park YM and Kim GY: Sulforaphane sensitizes tumor necrosis factor-related apoptosis-inducing ligand-mediated apoptosis through downregulation of ERK and Akt in lung adenocarcinoma A549 cells. Carcinogenesis 28: 1058-1066, 2007.
32. Chaudhuri D, Orsulic S and Ashok BT: Antiproliferative activity of sulforaphane in Akt-overexpressing ovarian cancer cells. Mol Cancer Ther 6: 334-345, 2007.

33. Bustany S, Cahu J, Guardiola P and Sola B: Cyclin D1 sensitizes myeloma cells to endoplasmic reticulum stress-mediated apoptosis by activating the unfolded protein response pathway. BMC Cancer 15: 262, 2015.
34. Kuroda Y, Sakai A, Tsuyama N, Katayama Y, Munemasa S, Asaoku H, Okikawa Y, Nakaju N, Mizuno M, Ogawa K, *et al*: Ectopic cyclin D1 overexpression increases chemosensitivity but not cell proliferation in multiple myeloma. Int J Oncol 33: 1201-1213, 2008.
35. Roué G, Pichereau V, Lincet H, Colomer D and Sola B: Cyclin D1 mediates resistance to apoptosis through upregulation of molecular chaperones and consequent redistribution of cell death regulators. Oncogene 27: 4909-4920, 2008.
36. Kim JE, Ryu HJ, Kim MJ and Kang TC: LIM kinase-2 induces programmed necrotic neuronal death via dysfunction of DRP1-mediated mitochondrial fission. Cell Death Differ 21: 1036-1049, 2014.
37. Zuryń A, Litwiniec A, Klimaszewska-Wiśniewska A, Nowak JM, Gackowska L, Myśliwiec BJ, Pawlik A and Grzanka A: Expression of cyclin D1 after treatment with doxorubicin in the HL-60 cell line. Cell Biol Int 38: 857-867, 2014.
38. Shankar S, Ganapathy S and Srivastava RK: Sulforaphane enhances the therapeutic potential of TRAIL in prostate cancer orthotopic model through regulation of apoptosis, metastasis, and angiogenesis. Clin Cancer Res 14: 6855-6866, 2008.
39. Shen G, Xu C, Chen C, Hebbar V and Kong AN: p53-independent G1 cell cycle arrest of human colon carcinoma cells HT-29 by sulforaphane is associated with induction of p21CIP1 and inhibition of expression of cyclin D1. Cancer Chemother Pharmacol 57: 317-327, 2006.
40. Yu J, Sun R, Zhao Z and Wang Y: *Auricularia polytricha* polysaccharides induce cell cycle arrest and apoptosis in human lung cancer A549 cells. Int J Biol Macromol 68: 67-71, 2014.
41. Zhang F, Zhang T, Teng ZH, Zhang R, Wang JB and Mei QB: Sensitization to gamma-irradiation-induced cell cycle arrest and apoptosis by the histone deacetylase inhibitor trichostatin A in non-small cell lung cancer (NSCLC) cells. Cancer Biol Ther 8: 823-831, 2009.
42. Lv XJ, Zhao LJ, Hao YQ, Su ZZ, Li JY, Du YW and Zhang J: Schisandrin B inhibits the proliferation of human lung adenocarcinoma A549 cells by inducing cycle arrest and apoptosis. Int J Clin Exp Med 8: 6926-6936, 2015.
43. Yuan L, Zhang Y, Xia J, Liu B, Zhang Q, Liu J, Luo L, Peng Z, Song Z and Zhu R: Resveratrol induces cell cycle arrest via a p53-independent pathway in A549 cells. Mol Med Rep 11: 2459-2464, 2015.
44. Sikdar S, Mukherjee A and Khuda-Bukhsh AR: Anti-lung cancer potential of pure esteric-glycoside condurangogenin A against nonsmall-cell lung cancer cells in vitro via p21/p53 mediated cell cycle modulation and DNA damage-induced apoptosis. Pharmacogn Mag 11 (Suppl 1): S73-S85, 2015.
45. Singh N, Nambiar D, Kale RK and Singh RP: Usnic acid inhibits growth and induces cell cycle arrest and apoptosis in human lung carcinoma A549 cells. Nutr Cancer 65 (Suppl 1): 36-43, 2013.
46. Liu Z, Sun M, Lu K, Liu J, Zhang M, Wu W, De W, Wang Z and Wang R: The long noncoding RNA HOTAIR contributes to cisplatin resistance of human lung adenocarcinoma cells via downregualtion of $p21^{WAF1/CIP1}$ expression. PLoS One 8: e77293, 2013.